RESEARCH ARTICLE   **OPEN ACCESS**

PARAMETRIC STUDY OF THE THERMAL BEHAVIOR OF COLD METAL TRANSFER WELDING WITH TITANIUM

Djoubeir Debbah[1], Mohamed Walid Azizi[2*] and Ibtissem Gasmi[3]

[1] Environmental Engineering and Technology Laboratory, Abdelhafid Boussouf University Center, P.O. Box 26, 43000, Mila, Algeria
[2] Advanced Technologies in Mechanical Production Research Laboratory (LRTAPM), Annaba University, P.O Box 12, 23000 Annaba, Algeria.
[3] Computer Science and Applied Mathematics Laboratory (LIMA), Chadli Bendjedid El Tarf University P.B. 73, 36000, El Tarf, Algeria.

[1] http://orcid.org 0009-0003-8797-2952 , [2] http://orcid.org/ 0000-0003-1066-740X , [3] https://orcid.org/0000-0002-8939-1727

Email: debbah.dj@centre-univ-mila.dz, *medwalid.azizi@centre-univ-mila.dz, ibtissem-gasmi@univ-eltarf.dz

ARTICLE INFO	ABSTRACT
	This work focused on enhancing the efficiency of thermal behavior in the application of Cold Metal Transfer (CMT), especially for welding tough metals like titanium, has the potential to significantly impact the field of welding technology. The investigation of the thermal behavior of CMT welding, carried out by means of parametric analysis, was a crucial step in this direction. This research, carried out with the assistance of numerical simulations with COMSOL Multiphysics, particularly emphasized crucial factors such as plate thickness and welding power. The significance of this study in advancing our understanding of additive manufacturing in welding is highlighted by the findings of the study. These results, which illustrate the effects of the specified influencing parameters through temperature distribution at various time intervals, 2D and 3D graphs depicting temperature evolution along the welding path, and the 2D temperature profile at (t = 5s) across different plate thicknesses, have the potential to revolutionize the field of welding technology and bring about exciting new possibilities.

I. INTRODUCTION

The CMT manufacturing process is a complex and intricate process that significantly influences the quality of the additively made component. This involves a complex interplay of multi-physical and transdisciplinary phenomena, necessitating a comprehensive study to fully comprehend the physics and material science at the core of this technology and to achieve meticulous control over the production process.

A variety of physical processes, such as heat transfer from the arc to the electrode wire, wire electrode melting, droplet formation, droplet deposition onto the substrate, and bead cooling and solidification, are at play and influence the entire process. Each of these procedures can significantly affect the performance and dimensional accuracy of the final product. It's important to note that numerous technical factors govern these operations, and several comprehensive studies have been conducted to investigate how these technological factors impact the geometry, surface morphology, and mechanical properties of additively fabricated products. The thoroughness of these studies reassures us about the reliability of the findings.

The mechanical properties of the cladding material are significantly impacted by the heat exchange that takes place both during and after the deposit process [1–3]. Research has revealed that CMT cladding provides a substantial advantage over conventional techniques. This advantage is performed by the utilization of lower processing temperatures, which ultimately leads to less thermal impacts on the materials that are being treated [4],[5]. When it comes to cladding, it's a matter of concern that it is vulnerable to oxidation when it is exposed to high temperatures. However, it has been confirmed that CMT cladding may be utilized to clad a variety of substrates, including cobalt [6],[7], nickel [8–11], aluminum [12],[13], and steel-based alloys [14].

With advancements in welding research, computational modeling techniques have become more effective for analyzing laser welding behavior [15]. The categorization of the simulation models for laser welding allows us to understand the aspects of the welding process [16]. The first one covers thermo-mechanical and thermo-metallurgical studies, while the second one outlines studies

that combine fluid dynamics with energy transfer. Convective heat transfer is not included in this model since fluid dynamics are not a part of it. Fixing this restriction could be as simple as changing the heat source or the material's conductivity.

A volumetric heat source is mostly used since, during the material joining process, it is situated in the keyhole where the laser-material interaction transpires and the weld pool is generated. So, instead of being at the front, the two-dimensional elements are in the back, which allows us to model the laser beam's path from front to back and show the melt pool's shape.[17] provide a quick way to change heat source model parameters to mimic Cold Metal Transfer (CMT) welded joint temperatures and distortions.

The approach uses RSM and FEM. A 3D elastic-plastic FEM model represents mechanical behaviour, whereas a 3D transient FEM model with a Goldak heat flux simulates thermal behaviour. Design of Experiments (DoE) simulations alter heat source settings for FEM models. The data are utilised to create temperature and distortion polynomial regression models. RSM automates pre- and post-processes and replaces trial and error to discover the ideal settings, reducing engineering time.

Cold Metal Transfer (CMT) is a variant of Gas Metal Arc Welding (GMAW) where molten metal is transferred to the weld pool primarily during the short-circuit phase, with the wire being retracted to allow precise, spatter-free welds with lower energy input. To simulate this process, a model using the Smoothed Particle Hydrodynamics (SPH) method was developed [18], addressing mass and heat transfer. A simplified surrogate model served as the arc heat source.

The SPH-based welding simulation model, with its inclusion of surface effects, Joule heating of the wire, and electromagnetic forces, demonstrates a high level of precision and reliability, as evidenced by its good qualitative agreement with real experiments.

A thermal source model for Cold Metal Transfer (CMT) welding has been developed to simulate the dynamic temperature field of the welding pool [19]. The model's predictions were validated by comparing the thermal cycle curve of 16Mn steel surfacing welding with experimental measurements using ANSYS finite element simulations. The results showed a significant agreement, confirming the model's reliability and providing reassurance about its accuracy. This analysis helps simplify CMT welding experiments and optimize process parameters.

Thermo-mechanical simulations, considering phase changes and the actual weld geometry induced by the filler material, were conducted using an equivalent heat source approach [20]. A unique heat exchange coefficient, accounting for thermal losses, was identified. By incorporating these losses into thermal calculations, a good agreement was found between measured and calculated temperatures.

The thoroughness of the mechanical calculations allowed for the recovery of the horse saddle shape after actual welding, with a relative difference of less than 10% in angular distortion between calculated and measured values, instilling confidence in the model's ability to predict mechanical behavior.

In cold metal transfer welding, periodic and recurrent arcing and metal deposition are simulated using a heat source model [21]. This model will enable detailed analysis of weld pool behaviour and mechanical characteristics for this welding.

The suggested model uses a double-ellipsoidal heat source model, which depicts the heat source as two ellipsoids, one for the arc and one for the droplet, and makes geometrical and heat input parameters time-dependent. The CMT welding process was used to obtain dissimilar welded joints of a super-austenitic stainless (AL6XN) and a nickel-based super alloy (IN718) [22]. Microhardness, tensile and low cycle fatigue tests were carried out to determine the mechanical behavior of the welded joints. The main purpose of this work is to analyze the low cycle fatigue behavior of dissimilar welded joint as well as the heat input effect of the CMT welding process. A 3-D transient thermal conduction finite element model was developed to correlate the thermal history with the microstructural transformation on the HAZ. This model was experimentally validated by weld thermal cycles obtained from K-type thermocouples [20] simulate CMT welding of thin stainless-steel sheets to predict temperature fields and welding-induced deformations. Instrumented tests and numerical simulations were established to compare experiments and simulations. Butt-welding stainless-steel sheets 1 to 1.2 mm thick were proposed.

To establish an analogous heat source for each arrangement, weld seam samples were inspected. Electric current, voltage, and K-type thermocouples were also measured. Additional displacement measurements were made utilizing DIC (Digital Image Correlation). Then, thermomechanical simulations were performed using an equivalent heat source technique, taking into account element phase shifts from solid to liquid and liquid to solid. These models additionally incorporate filler-induced [23] evaluate CMT technology's history, variations, improvements, and prospects. The research begins by tracing the history of CMT welding and the introduction of many versions with different properties and uses.

Recent CMT process parameter optimization studies have improved weld quality and productivity, improving parameter control, arc stability, and wire feeding mechanisms. Research has also examined the microstructural development and mechanical characteristics of CMT welded joints for comparable and dissimilar metals, revealing material compatibility, joint design, and performance under different situations. CMT technique has been shown to be versatile in Laser-CMT hybrid welding, CMT cladding, CMT wire arc additive manufacturing, and CMT welding for repair across materials.

This study significantly enhances the understanding of the thermal processes involved in the CMT welding process on titanium for linear applications, a crucial area in the field of welding and materials science. Utilising COMSOL Multiphysics simulations, we examined the heat exchange during welding, with special emphasis on the motion and deformation of the metal droplet.

This enabled us to get significant insights into the thermal processes happening throughout the welding process. Furthermore, we analysed the influence of critical process factors, including workpiece thickness and applied electrical power, on temperature distribution and thermal dynamics. The simulations evaluated three workpiece thicknesses (2 mm and 5 mm) and three levels of applied electrical power (800W, 850W, and 900W).

The findings are displayed as temperature distribution at various time intervals, accompanied by 2D and 3D graphs that depict the temperature progression throughout the welding route. Additionally, we presented a comprehensive 2D temperature profile at a designated time (t=5s) across different plate thicknesses.

The present investigation enhances comprehension of the impact of process factors on the thermal field in linear welding, which is crucial for optimising welding parameters, mitigating faults, and improving the overall quality of the welded material.

II. NUMERICAL MODELING

II.1 WELDING OF METAL PLATE

The complete modeling of thermal processes involving electric arcs and molten pools is highly complex, requiring consideration of various factors like thermo-fluid heat transfers and electromagnetic phenomena. While extensive literature exists on modeling these aspects, our study simplifies by focusing solely on heat conduction. We replace the intricate details of the arc and molten pool with a simplified heat source. While this approach provides insights, it's important to acknowledge its limitations in accurately representing the system.

II.1.1 HYPOTHESES

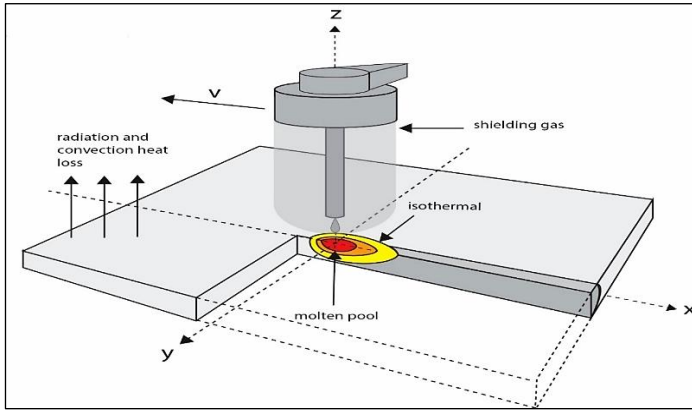To study and model heat transfers during a welding (Figure 1), hypotheses are required:

Figure 1: The welding process of two thin sheets.
Source: Authors, (2025).

1-The 3D axi-symmetric heat transfer problem (ABFE plane of symmetry),
2-Throughout the study, it is assumed that the heat source is moving. Al though complex paths of the source can be considered, we place ourselves in the case of a rectilinear translation at constant speed along an axis in Cartesian coordinates (case of plate welding).
3-The regime is considered Transitional,
4- The X axis coincides with the welding direction
5- The physical properties of the material are considered constant.
6-The flow in the weld pool and the electromagnetic phenomena (the forces of gravity (buoyancy), surface tensions (Marangoni forces), viscosity of the liquid metal, aerodynamic shear, electromagnetic forces (Lorentz forces)) are considered negligible.
7-Heat losses by convection and radiation through free surfaces and the boundaries of the room are taken into account.

II.1.2 HEAT GOVERNING EQUATION

The heat conduction equation in the domain Ω (domain defined by the two metal plates to weld) (Figure 1) is written for the three-dimensional case.

$$\rho c_p \frac{\partial(T)}{\partial t} = \frac{\partial}{\partial x}\left(K \frac{\partial T}{\partial x}\right) + \frac{\partial}{\partial y}\left(K \frac{\partial T}{\partial y}\right) + \frac{\partial}{\partial z}\left(K \frac{\partial T}{\partial z}\right) + S \qquad (1)$$

Where T is the temperature, t the time, ρ the density of the material to be welded, Cp the specific heat, K the thermal conductivity and S the heat generated or absorbed per unit of time.
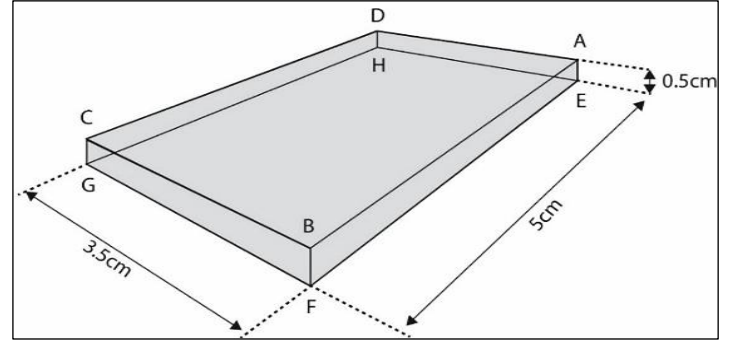

Figure 2: Ω domain and boundaries.
Source: Authors, (2025).

The general form of the equation above is:

$$\rho c_p \frac{\partial T}{\partial t} = -div\left(-K\overrightarrow{grad\,T}\right) + S \qquad (2)$$

The solution of this equation gives the temperature distribution in the domain Ω, that means the change in temperature with relative to the change in position and time.

II.1.3 BOUNDARY AND INITIAL CONDITIONS

The boundary conditions are determined from the equations of the heat flow exchanged with the surrounding environment by convection and radiation.
1) The energy given by the electric arc is modeled by a heat source S which is moves with a speed v along the x axis, this heat flux is q is transmitted to the plate through the upper face (ABCD).

$$q_n = S - [h_\infty(T - T_\infty) + \sigma\varepsilon(T^4 - T_\infty^4)] \qquad (3)$$

1) At the borders (ADHE), (DCGH), (BCGF) and (EFGH) (Figure 2), the flow qn is equal to:

$$q_n = h_\infty(T - T_\infty) + \sigma\varepsilon(T^4 - T_\infty^4) \qquad (4)$$

Were
h∞: convection coefficient.
T: temperature at the edge of the assembly (K).
T∞: ambient temperature (K).
ε: thermal emissivity.
σ: Boltzmann constant equal to $5.67.10^{-8} w/m^2 K^4$.
1) In the symmetry plan (ABFE), the heat flow is zero:

$$q_n = -K \frac{\partial T}{\partial x} = 0 \qquad (5)$$

2) The initial temperature of the material is assumed equal to the ambient temperature.

II.1.4 FINAL EQUATIONS SYSTEM

We have the three following equations:

$$\rho c_p \frac{\partial(T)}{\partial t} = \frac{\partial}{\partial x}\left(K \frac{\partial T}{\partial x}\right) + \frac{\partial}{\partial y}\left(K \frac{\partial T}{\partial y}\right) + \frac{\partial}{\partial z}\left(K \frac{\partial T}{\partial z}\right) + S \qquad (6)$$

$$q_n = S - [h_\infty(T - T_\infty) + \sigma\varepsilon(T^4 - T_\infty^4)]$$
$$in\ (ADHE), (DCGH), (BCGF) and\ (EFGH) \qquad (7)$$

$$q_n = 0\ in\ (ABFE) \qquad (8)$$

The source term S will be modeled subsequently to close the system of equations. The equation the final differential is therefore a nonlinear partial differential equation.

II.1.5 HEAT SOURCE MODELS

In our study, the heat source model used is The Goldak Double-Ellipsoid Heat Source. Were the center point of the weld arc moves along the x axis, at a velocity v. Its current position is thus given by x0 = v.t. The heat source by Goldak is defined by two regions that join at x0, and whose shapes are ellipsoidal. The widths α and depths b of these regions are equal, but the front and rear lengths, c_f and c_r, may differ, see Figure 3. The heat source is given by:

$$q_v = \begin{cases} Q_m . e^{\left(-3\left[\frac{(x-x_0)^2}{c_f^2}+\frac{y^2}{a^2}+\frac{z^2}{b^2}\right]\right)} & (x \geq x_0) \\ Q_m . e^{\left(-3\left[\frac{(x-x_0)^2}{c_r^2}+\frac{y^2}{a^2}+\frac{z^2}{b^2}\right]\right)} & (x < x_0) \end{cases} \tag{9}$$

where Q_m as mentioned in chapter one is the power density of the weld, given by:

$$Q_m = \frac{6\sqrt{3}.Q_0 f_r}{c_r bc\pi\sqrt{\pi}} = \frac{6\sqrt{3}.Q_0 f_f}{c_f bc\pi\sqrt{\pi}} \tag{10}$$
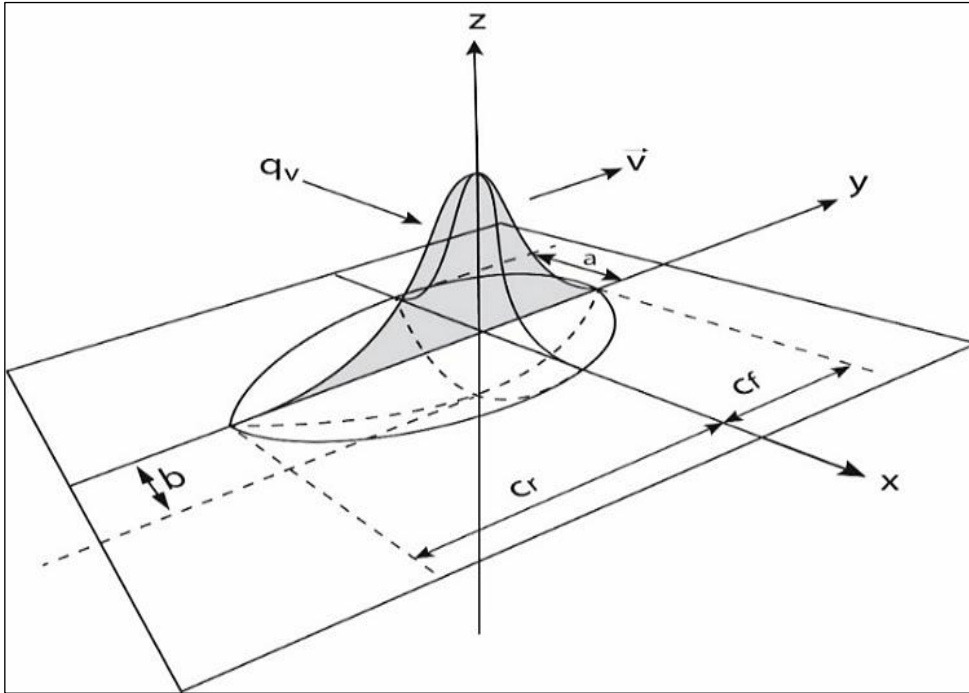

Figure 3: 3D double-ellipsoid heat sources.
Source: Authors, (2025).

II.1.6 PULSING EFFECT

The pulsing effect is the result of the automatic current cut each time a drop of melting feeding wire is in touch with the molten pool causing a short circuit, the modeling of this effect required the integration of a periodic function β into the moving heat source heat flux equation.

$$q(n)_{pulsed} = q(n).\beta \tag{11}$$

Were $\quad \beta = rect1\left(mod\left(t[s],\frac{1}{f}\right)\right) \tag{12}$

Were f is the frequency of the pulsing, rect1 is the COMSOL rectangular pulse function module and mod is the COMSOL command that create the repetition of the pulse every $(1/f)$ step in time t.

II.3 MATERIALS

The materials used in this simulation are the titanium grade one alloy, aluminum 1050 alloy and the ARMCO iron alloy. The thermal properties such as thermal conductivity, heat capacity, and materials density will be taken from the COMSOL material library.

II.4 PROPERTIES

All the properties needed are gathered in the Table 1.

Table 1: Simulation properties.

Symbol	Value	Description
Lx	0.05m	Plate length
L_y	0.035m	Plate width
L_z	0.005m /0.002m /0.008m	Plate thickness
Q_0	800W /850W /900W	Weld power
v	0.001m/s	Welding speed
A	0.004m	Goldak ellipsoid measurement
B	0.004m	Goldak ellipsoid depth
c_r	0.008m	Goldak ellipsoid length, rear
c_f	0.004m	Goldak ellipsoid, front
f_r	1.3333	Goldak parameter
f_f	0.66667	Goldak parameter
F	50Hz	Pulse frequency
ε	0.4	emissivity
h	10W/m^2.K	Convective heat transfer coefficient

Source: Authors, (2025).

III RESULTS AND DISCUSSIONS

III.1. WELDING OF METAL PLATE RESULTS

This simulation aimed to study the results of changing different parameters such as plate thickness, welding power and plate material on the temperature distribution and how its behave during CMT welding.

III.1.1 MESHING EFFECT

The more refined the mesh the more accurate the results with a smooth Gaussian curve transition of temperature value from a point to the next one indicating a mush realistic change in the temperature gradient. Based on that the extremely fine mesh is chosen with a 142669 tetrahedral element, 10312 triangular face and 360 edge elements (Figure 4).
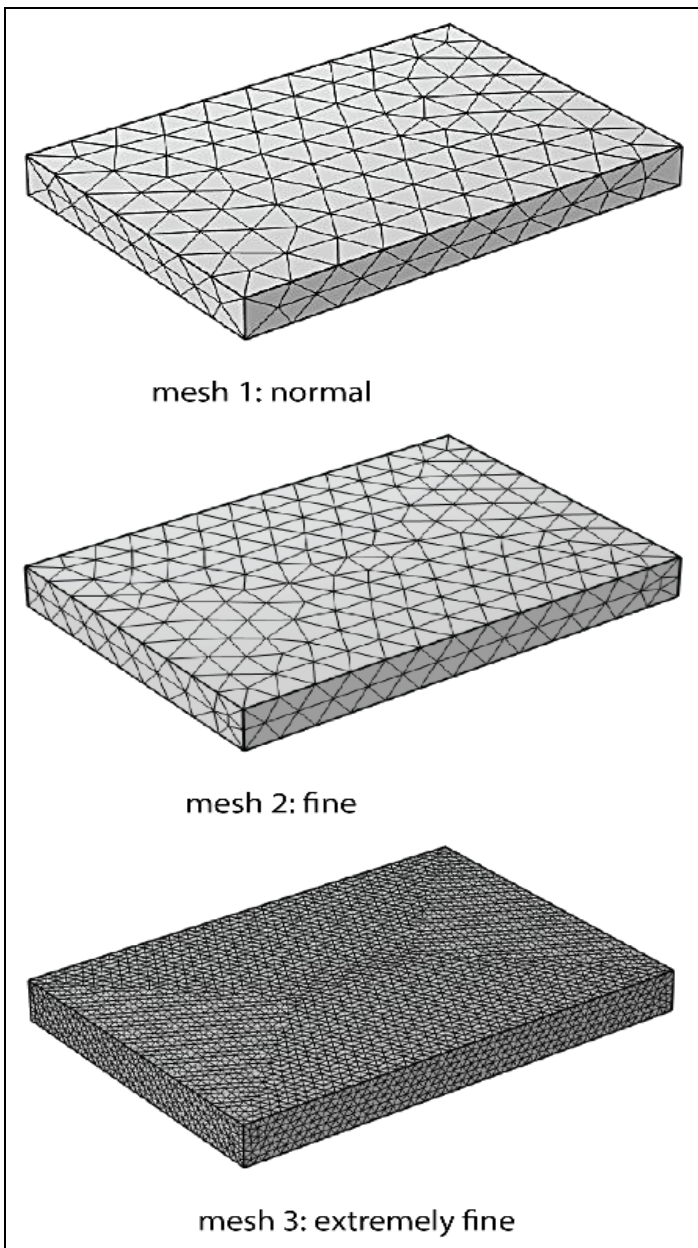
Figure 4: Different mesh types.
Source: Authors, (2025).

Figure 5 demonstrates the efficiency of more granulated meshes in temperature simulations. These meshes, while less detailed, are more cost-effective in terms of computational resources. On the other hand, finer meshes, while offering more precision, require a greater portion of computational welding resources.
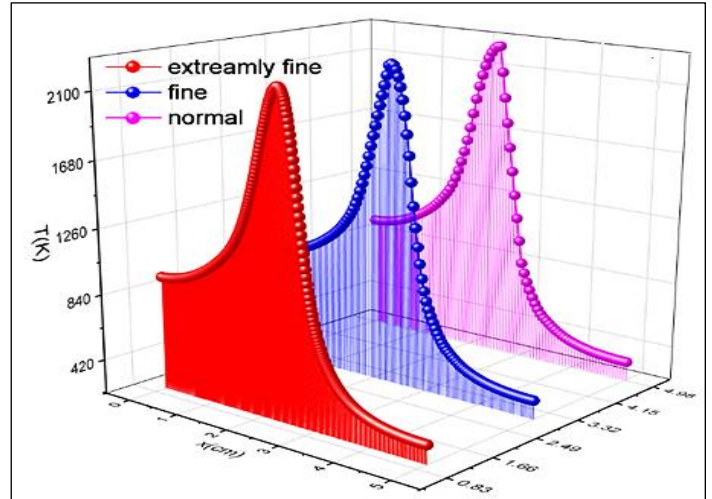

Figure 5: Temperature distribution for three mesh types.
Source: Authors, (2025).

III.1.2 INFLUENCE OF PLATE THICKNESS ON TEMPERATURE DISTRIBUTION

The temperature profile of a titanium plate subjected to a continuous 800W power input during welding is shown in Figure 6. At the beginning of the time steps, it shows the heat concentration in the welding zone, and as time goes on, it spreads, making a temperature gradient. Understanding the heat-affected zones and maintaining material integrity during welding are both aided by the dynamic variations in the temperature distribution.
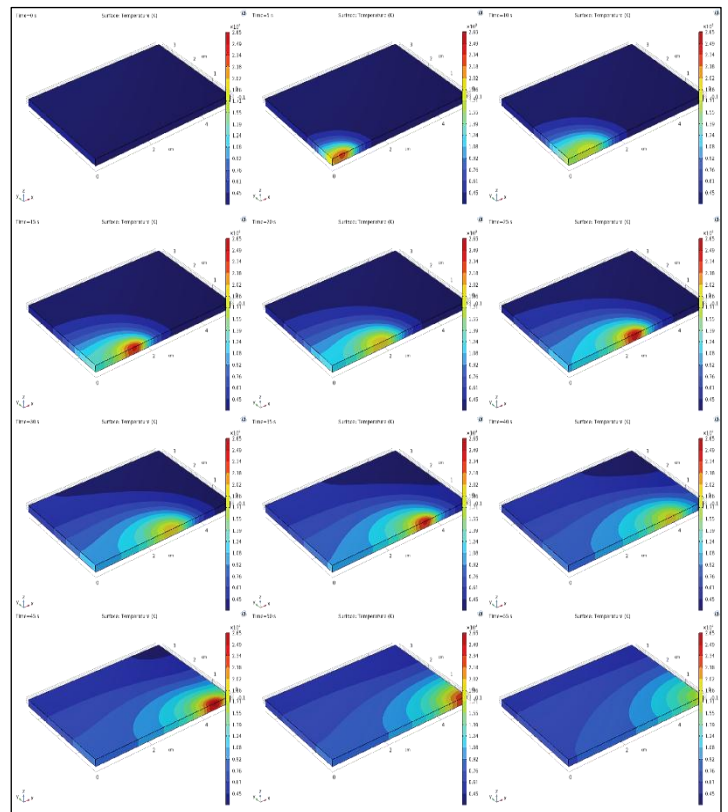

Figure 6: Temperature distribution in a 2mm height titanium plate in different time steps with 800W welding power.
Source: Authors, (2025).

Figure 7 depicts the temperature fluctuations along the titanium welding route over time. With a continuous 800W welding power, the 3D plot displays the surface and depth temperature distribution of the 2mm-thick plate. The welding process generates heat that propagates along the line, creating a shifting high-temperature zone. The x and y axes show the welding path's position on the surface and across the plate's thickness, while the z-axis displays the temperature at different time intervals. Time steps demonstrate how heat diffuses from the original weld location, forming a progressive heat-affected zone. High and low temperatures throughout the welding route are clearly visible in 3D.
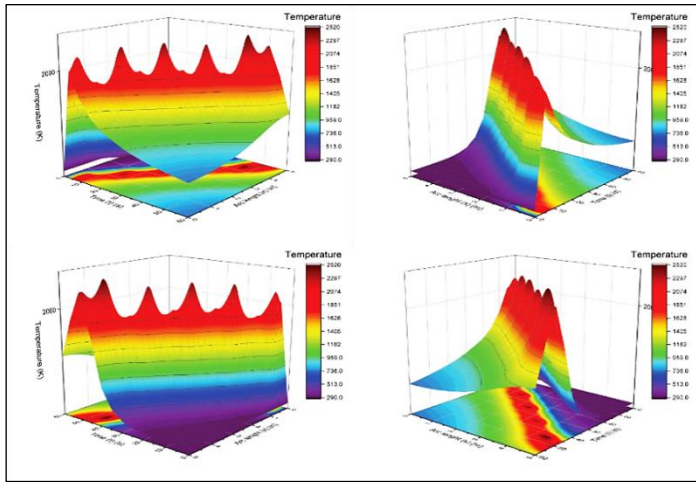

Figure 7: 3D graphic representation temperature evolution along the welding path at different time steps in a 2mm height titanium plate with 800W welding power.
Source: Authors, (2025).

Figure 8 presents a two-dimensional visualization of the temperature distribution along the welding path over time. The graph likely plots the temperature along the surface of the titanium plate at various time intervals, with the x-axis representing the position along the welding path and the y-axis showing the temperature at different points along that path. The welding power, under our precise control, is fixed at 800W, ensuring a consistent heat application. As the welding progresses, heat is applied to the plate, causing a temperature rise near the weld zone. As time progresses, the heat spreads from the centre of the weld, creating a temperature gradient that gradually decreases as the distance from the weld increases.
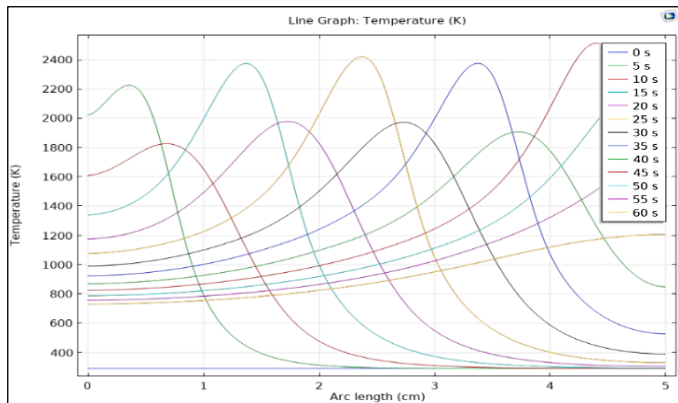

Figure 8: 2D graphic representation temperature evolution along the welding path at different time steps in a 2mm height titanium plate with 800W welding power.
Source: Authors, (2025).

The progression of temperature within a titanium plate with a thickness of 5 mm is depicted in Figure 9, which describes the welding process conducted with a constant power input of 800 watts. The temperature distribution is displayed across a number of time steps, which demonstrates how the heat that is created by the welding process travels through the material.

As a result of the focused heat that is applied by the welding arc, the temperature closest to the welding spot is at its greatest during the first step. With time, the heat will eventually travel throughout the plate, resulting in the formation of a thermal gradient that will expand away from the weld zone. Thermal conduction is the cause of this heat diffusion, which occurs when heat moves from regions with higher temperatures to areas with lower temperatures, resulting in the formation of a heat-affected zone (HAZ).

As a result of the plate's increased thickness (5mm) in comparison to thinner plates, the temperature gradient is likely to become more noticeable, with a more progressive fall in temperature further away from the weld. The titanium plate must be protected from heat deformation while still maintaining its structural integrity.
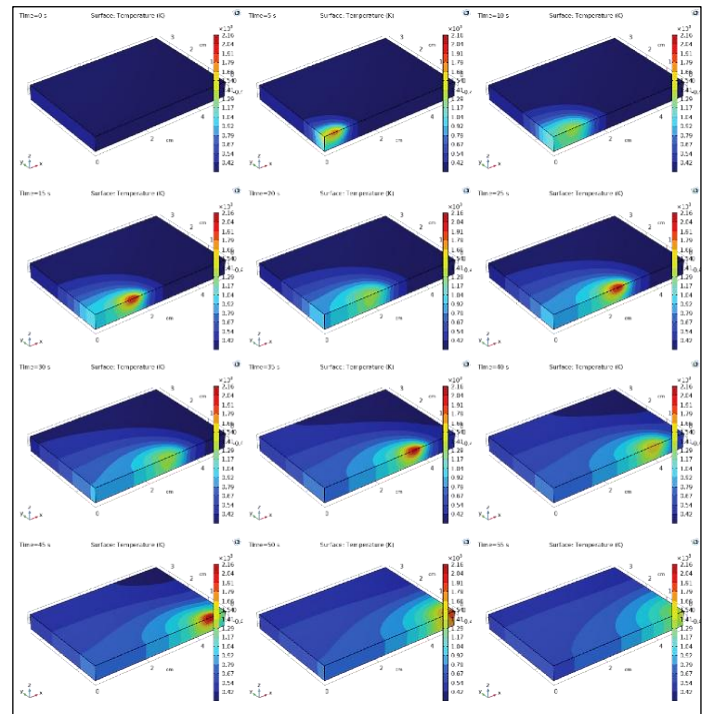

Figure 9: Temperature distribution in a 5mm height titanium plate in different time steps with 800W welding power.
Source: Authors, (2025).

Figure 10 shows the welding path temperature distribution over time in three dimensions. The z-axis shows temperature at different time steps, while the x and y axes presumably depict location along the surface and potentially across the depth of the 5mm-thick titanium plate. Since the welding power is 800W, the heat created by the welding arc first concentrates at the weld spot, raising the temperature sharply there.

Heat propagates throughout the plate's surface and thickness, forming a complicated thermal gradient over time. A growing heat-affected zone (HAZ) forms when heat diffuses through the plate, as seen in the picture. The 5mm thickness absorbs and transmits thermal energy. Thus, the vertical temperature gradient is greater, and the heat distribution is slower than with thinner plates.
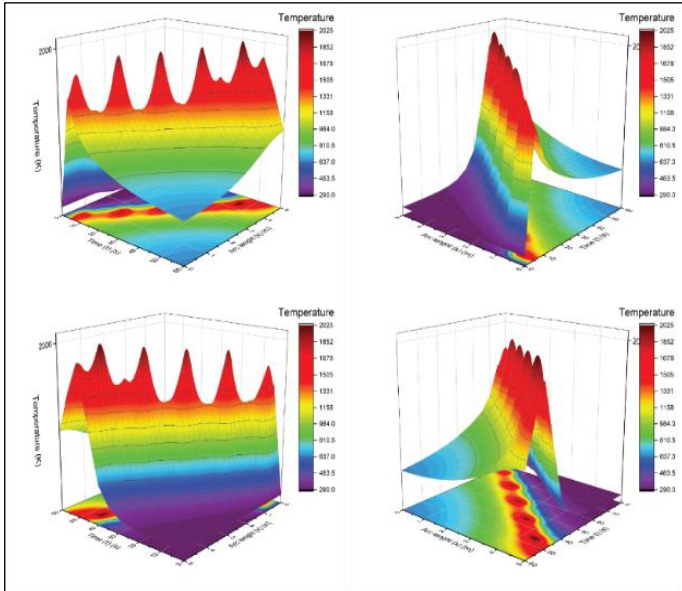
Figure 10: 3D graphic representation temperature evolution along the welding path at different time steps in a 5mm height titanium plate with 800W welding power.
Source: Authors, (2025).

Figure 11 depicts a 5mm-thick titanium plate's welding route temperature with time in two dimensions. When the welding power is 800W, the weld zone temperature is maximum due to the welding arc's focused heat. A thermal gradient, which is the rate of temperature change over a unit distance, forms when heat diffuses over the plate's surface and depth. Heat flows through the material, expanding the heat-affected zone (HAZ) and reducing the temperature as it goes away from the weld. Due to the plate's 5mm thickness, the temperature gradient would be greater and take longer to disperse.
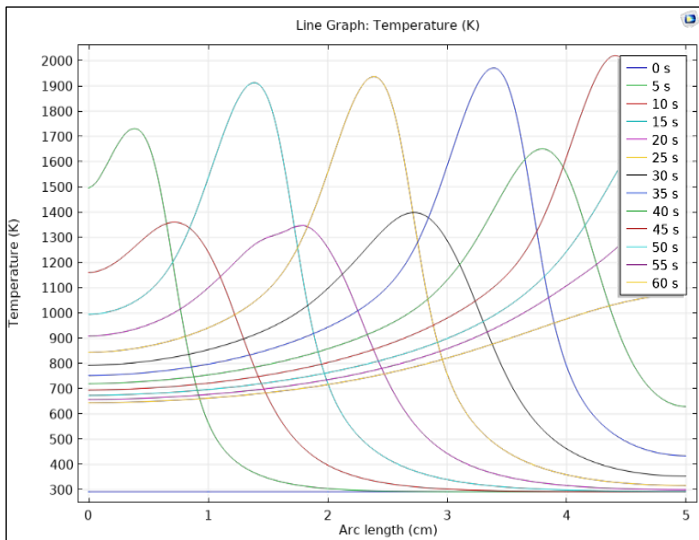

Figure 11: 2D graphic representation temperature evolution along the welding path at different time steps in a 5mm heigh titanium plate with 800W welding power.
Source: Authors, (2025).

Figure 12 illustrates how the modest temperature gradient on the 2 mm thick plate allows heat to swiftly diffuse, while the 5 mm and 8 mm thick plates present different challenges. The heat takes longer to permeate through the 5 mm thick plate,

causing a greater temperature gradient and a higher heat effect. The 8 mm thick plate has a higher thermal barrier to heat diffusion, resulting in a more localized heat distribution and a deeper temperature gradient. This comparison underscores the critical role of plate thickness in heat propagation, HAZ size, and cooling rate. By adapting welding settings for various workpiece thicknesses, we can optimize material qualities, reduce overheating, and minimize plate distortions and stresses, offering a hopeful outlook for our work.
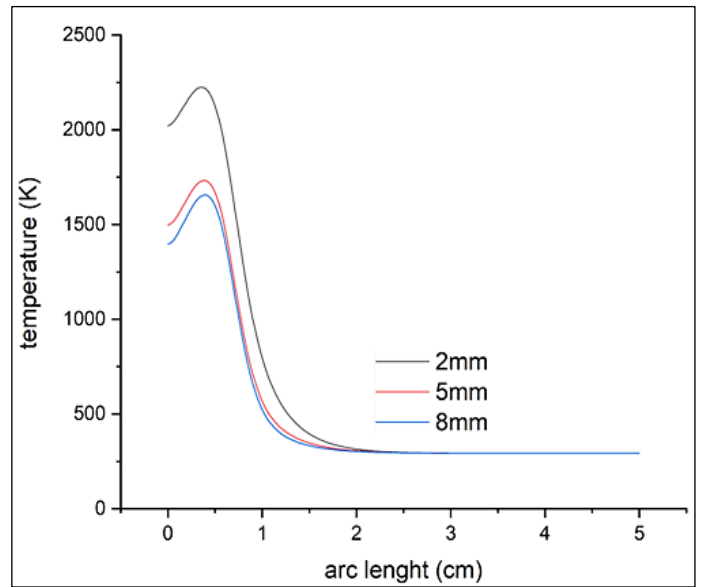

Figure 12: 2D graphic representation of temperature evolution along the welding path at t=5s in the different thickness plates.
Source: Authors, (2025).

III.1.2 INFLUENCE OF WELDING POWER ON

The simulations of temperature distribution show distinct differences at welding powers of 800 watts and 900 watts. Figure 13 illustrates the dynamic heat transfer that takes place throughout the welding process by showing the temperature distribution within the plate. First, there is a sharp concentration of heat at the weld zone, which raises the temperature quickly and locally.

There is a noticeable temperature gradient between the hot weld zone and the colder surrounding material because titanium's comparatively poor thermal conductivity prevents heat from spreading rapidly.

Due to the material's poor heat conductivity, the heat does not diffuse more uniformly throughout the plate. Therefore, this concentration of heat stays close to the weld for a long time. But as time goes on, the heat starts to permeate the material's depth as well as the plate's surface. Because titanium resists heat flow, this diffusion happens more slowly in the deeper areas of the plate, but it still occurs gradually over time.

The slow spread of heat creates a heat-affected zone (HAZ), which becomes larger as the welding process continues. The area where the material has seen a rise in temperature but has not melted is represented by the HAZ.

A larger HAZ is possible with a 5 mm thick plate because the heat is held in place longer than with thinner plates. This prolonged heat retention in thicker plates significantly impacts the welding process, as it leads to a more even and prolonged heating, potentially altering the material's hardness and microstructure in the heat-affected area.
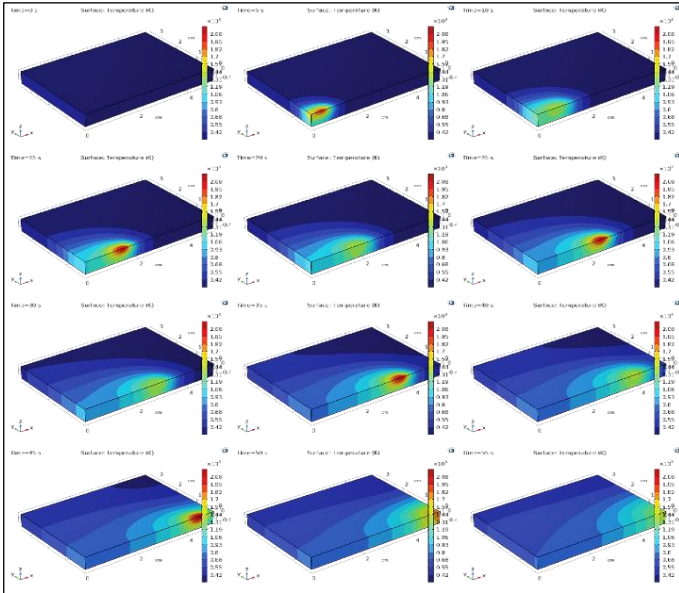
Figure 13: Temperature distribution in a 5mm height titanium plate in different time steps with 850W.
Source: Authors, (2025).

Figure 14 provides a 3D visualization of the temperature evolution along a 5mm thick titanium plate during welding with 850W power. It's a practical tool that allows us to see how heat is first concentrated in the weld zone, leading to a rapid temperature rise. The model also demonstrates how the poor thermal conductivity of titanium slows heat diffusion from the weld into the plate. As heat spreads, the HAZ expands, and the temperature drops from the weld spot. This practical visualization is crucial for optimizing welding conditions and managing material qualities, as it shows how the HAZ expands and how heat affects the plate's surface and interior.
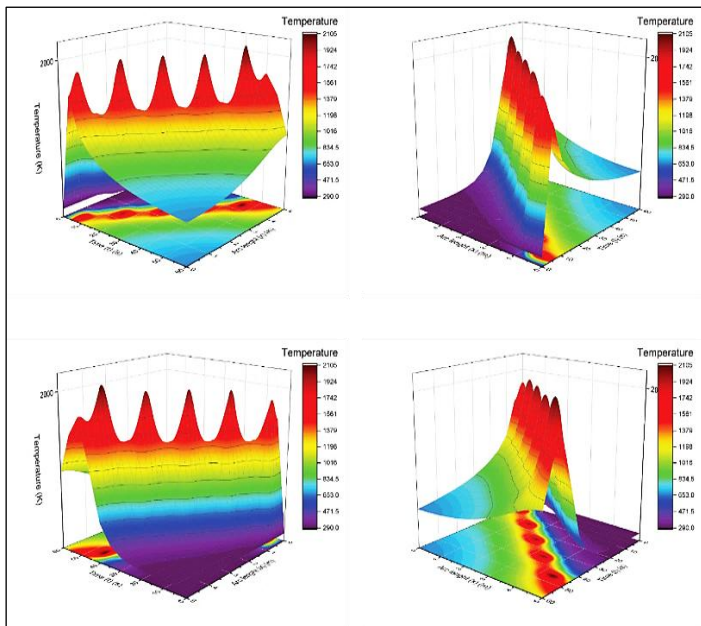

Figure 14: 3D graphic representation of temperature evolution along the welding path at different time steps in a 5mm height titanium plate with 850W welding power
Source: Authors, (2025).

Figure 15 shows the temperature distribution throughout a 5 mm-high titanium plate during welding at various time intervals. The key factor in this process is the 850W welding power, which

uniformly raises the temperature. The heat from the welding source increases the temperature throughout the route, with the greatest temperatures around the weld bead centre. The graph represents the temperature gradient as heat drains from the weld zone over time. Direct heat input first raises the temperature around the welding area while the surrounding regions gradually cool. The time steps show how the thermal profile varies during welding, indicating the material's reaction to applied heat and plate conductive, convective, and radiative heat losses.
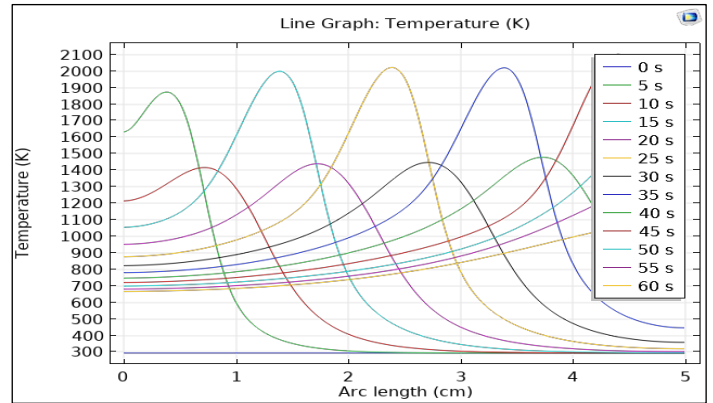

Figure 15: 2D graphic representation temperature evolution along the welding path at different time steps in a 5mm height titanium plate with 850W welding power.
Source: Authors, (2025).

Figure 16 shows the temperature distribution over a titanium plate that is 5 mm thick when welding at a power of 900W. Heat diffusion and the strength of the thermal gradient within the material are shown in the picture, which also illustrates the temperature's evolution over time.
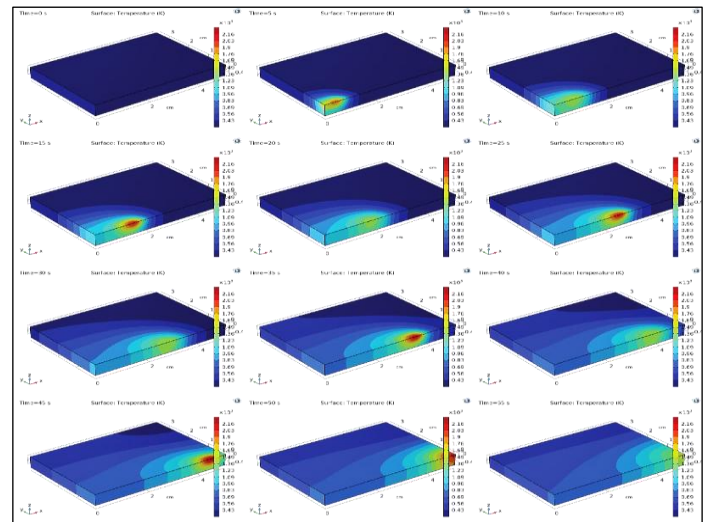

Figure 16: Temperature distribution in a 5mm height titanium plate in different time steps with 900W welding power.
Source: Authors, (2025).

In the first-time step, there is a strong temperature differential between the weld site and the colder areas outside it, and the heat is focused there. A more consistent temperature distribution is achieved as time goes on because the heat dissipates throughout the whole plate. Closer to the weld, however, the temperature stays higher, suggesting that heat is still escaping from the spot. The picture depicts many time steps, showing how the material cools down progressively as heat is transferred away

from the weld zone. An essential component in deciding the quality of the weld and avoiding thermal distortion or damage is the material's capacity to transmit and disperse heat; the overall distribution of temperatures reflects this. The 900W welding power indicates a rather high energy input.

Figure 17 shows the temperature change throughout the welding route in a 5 mm titanium plate exposed to 900W welding power at various time intervals. The highest point on the temperature curve, the welding spot, concentrates heat at the start of the welding process.

Heat diffuses down the plate's surface and depth over time, providing a thermal gradient that diminishes as it goes away from the welding path. Heat flow is dynamic, and the 3D graphic shows spatial and temporal temperature variations.

The temperature may be represented by colour intensity or surface height, with hotter areas near the weld and colder regions further away. Slowly flattening the temperature surface shows that the material is cooling and the welding operation has less thermal impact, which refers to the reduction in the heat's influence on the material.

This image shows how heat conduction, material qualities, and welding factors like power interact, making it essential for managing heat to achieve ideal weld quality without destroying the titanium plate.
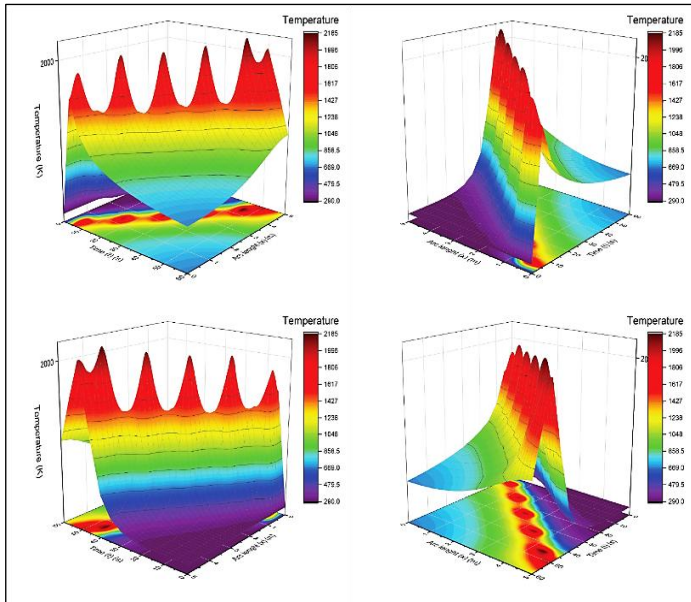

Figure 17: 3D graphic representation of temperature evolution along the welding path at different time steps in a 5mm height titanium plate with 900W welding power.
Source: Authors, (2025).

The temperature change across the welding route in a titanium plate that is 5 mm thick and exposed to 900W of welding power at different time intervals is shown in Figure 17. The greatest temperatures initially concentrated at the weld site correspond to the region where the heat is most intense, and the graph shows how the temperature fluctuates as the welding process proceeds.

Position along the welding line is probably represented by the x-axis, while the y-axis shows temperature. The weld zone is noticeably hotter than the surrounding material at early time steps, resulting in a sharp temperature gradient.

The heat, in a predictable and gradual manner, starts to disperse, and as the heat penetrates the material, the temperature profile along the welding route flattens. At subsequent time steps,

the temperature is distributed more uniformly across the plate because the regions farthest from the weld zone cool more rapidly.
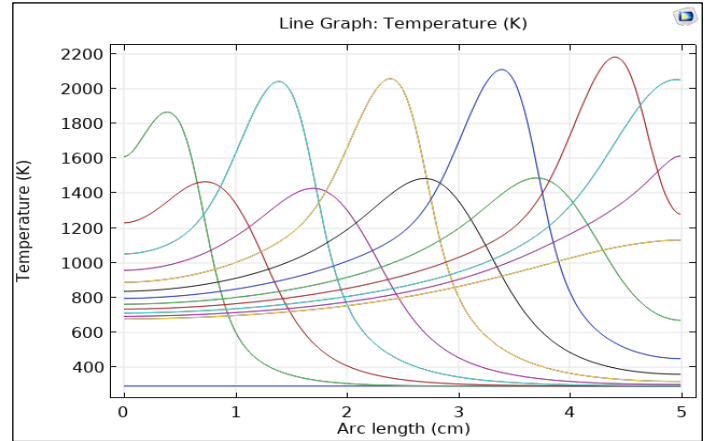

Figure 18: 2D graphic representation temperature evolution along the welding path at different time steps in a 5mm height titanium plate with 900W welding power.
Source: Authors, (2025).

Figure 19 shows volume displacement magnitude distribution within a 5 mm-thick titanium plate subjected to 800W welding power over time. During welding, the material absorbs heat and expands, as seen in the graph. In the first-time step, displacement is localized near the welding site, where the temperature is highest. Heat spreads over the plate during

welding, causing thermal expansion and displacement away from the weld zone. The material adjacent to the weld deforms more when heated and expanded, whereas colder portions further away deform less. The plate cools, reducing displacement with time. The graphic shows how the 800W welding power's temperature gradient affects the material's mechanical response, demonstrating the importance of welding power and heat dispersion in deformation.
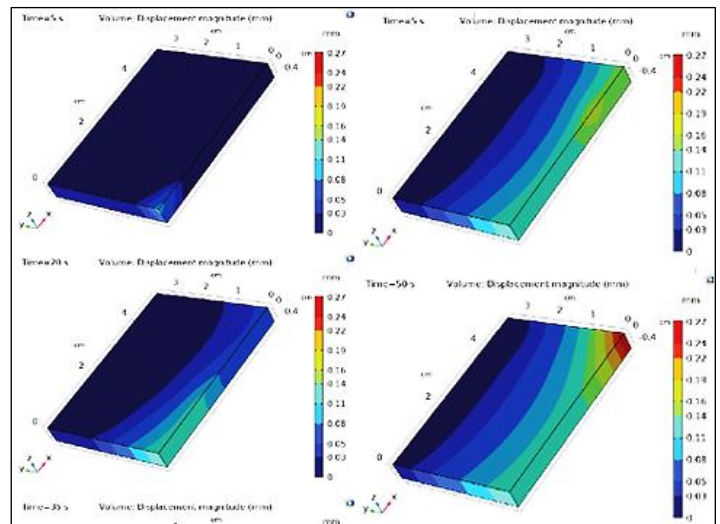

Figure 19: Volume displacement magnitude distribution in a 5mm height titanium plate in different time steps with 800W welding power
Source: Authors, (2025).

Figure 20 illustrates the distribution of volume displacement magnitude inside a 5 mm-thick titanium plate at various time intervals subjected to an 800W welding power. This research has practical implications, as it helps us understand the

material's deformation during the welding process. Titanium Grade 1, with its poor heat conductivity, exhibits significant localized deformation, especially near the welding site. Thermal accumulation in the welding area induces thermal expansion, leading to material deformation.

The maximum displacement reaches 0.26 mm, indicating considerable expansion at the weld zone. The limited heat dispersion, due to the restricted thermal conductivity of Titanium Grade 1, creates a steep temperature gradient, causing localized thermal expansion around the weld region. As time progresses and the heat dissipates, the degree of displacement diminishes.

This localized deformation is crucial for anticipating potential issues like residual strains or warping, which can impact the ultimate quality and structural integrity of the weld. The graphic effectively demonstrates the influence of welding parameters, especially the applied power, on the material's thermal and mechanical behaviour, underscoring the importance of regulating heat distribution to minimize undesirable deformations.
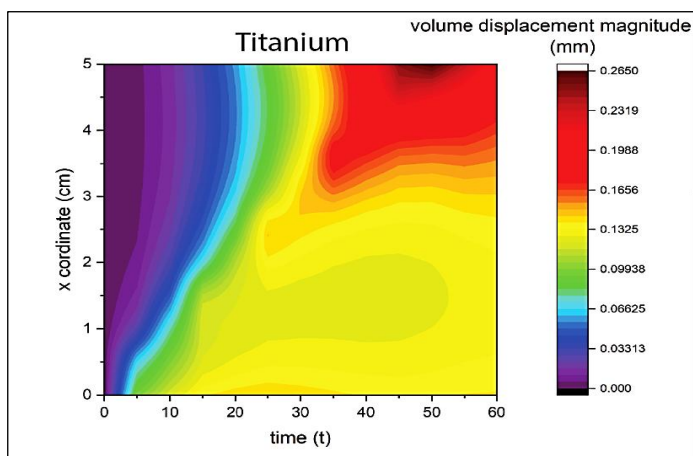

Figure 20: Volume displacement magnitude distribution in a 5mm height titanium, along the welding path in different time steps with 800W welding power.
Source: Authors, (2025).

IV. CONCLUSIONS

This study examined the thermal behaviour of Cold Metal Transfer (CMT) welding by numerical simulations using COMSOL Multiphysics. The thickness of the plate and the welding power were two critical factors on which we concentrated. The ramifications of our results, which underscore the need for meticulous control over welding conditions, might significantly impact welding practices in industrial environments.

Due to their reduced thermal mass, smaller plates (2mm) reached peak temperatures more swiftly than larger plates (5mm and 8mm), which absorbed greater amounts of heat and exhibited slower heating rates. We found that bigger plates absorbed greater amounts of heat and exhibited slower heating rates.

The maximum temperatures and heat-affected areas expanded when the welding power was raised from 800W to 900W. This was particularly evident in the 5mm thick titanium plate. Engineers may enhance weld quality by reducing thermal stresses and distortions, use these insights to adjust welding parameters for various power levels and material thicknesses.

The results underscore the industrial importance of CMT welding, especially in the automotive and aerospace sectors, due to its ability to join incompatible metals with little deformation and spatter. This competency is especially advantageous in the aviation sector. This extensive understanding of thermal behaviour in CMT welding, supported by numerical data and simulations, underscores the importance of optimizing parameters and selecting suitable materials to attain high-quality welds, thereby enhancing industrial welding practices.

VI. AUTHOR'S CONTRIBUTION

Conceptualization: Debbah Djoubeir.
Methodology: Debbah Djoubeir and Mohamed Walid Azizi.
Investigation: Debbah Djoubeir and Mohamed Walid Azizi.
Discussion of results: Debbah Djoubeir and Mohamed Walid Azizi.
Writing – Original Draft: Debbah Djoubeir, Mohamed Walid Azizi and Ibtissem Gasmi.
Writing – Review and Editing: Debbah Djoubeir, Mohamed Walid Azizi and Ibtissem Gasmi.
Resources: Debbah Djoubeir and Mohamed Walid Azizi.
Supervision: Mohamed Walid Azizi and Ibtissem Gasmi.
Approval of the final text: Debbah Djoubeir, Mohamed Walid Azizi and Ibtissem Gasmi.

VII. ACKNOWLEDGMENTS

V. REFERENCES

[1] G. H. S. F. L. Carvalho, G. Venturini, G. Campatelli, E. Galvanetto, "Development of optimal deposition strategies for cladding of Inconel 625 on carbon steel using Wire Arc Additive manufacturing," Surf. Coat. Technol., vol. 453, p. 129128, 2023.

[2] T. B. Thiagarajan, D. Raguraman, S. Ponnusamy, "Optimization of CMT welding parameters of Stellite-6 on AISI316L alloy using TOPSIS method," IJIE, vol. 15, pp. 161–172, 2023.

[3] H. Raushan, A. Bansal, V. Singh, A. K. Singla, J. Singla, A. Omer, J. Singh, D. K. Goyal, N. Khanna, R. S. Rooprai, "Dry sliding and slurry abrasion behaviour of Wire Arc Additive manufacturing – cold metal transfer (WAAM-CMT) cladded Inconel 625 on EN8 steel," Tribol. Int., vol. 179, p. 108176, 2023.

[4] Bunaziv, X. Ren, A. B. Hagen, E. W. Hovig, I. Jevremovic, S. G. Dahl, "Laser beam remelting of stainless-steel plate for cladding and comparison with conventional CMT process," Int. J. Adv. Manuf. Technol., vol. 127, pp. 911–934, 2023.

[5] S. Selvi, A. Vishvaksenan, E. Rajasekhar, "Cold metal transfer (CMT) technology - an overview," Defence Technology, vol. 14, no. 1, pp. 28–44, 2018.

[6] G. P. Rajeev, M. Kamaraj, R. S. Bakshi, "Comparison of microstructure, dilution and wear behavior of Stellite 21 hardfacing on H13 steel using cold metal transfer and plasma transferred arc welding processes," Surf. Coat. Technol., vol. 375, pp. 383–394, 2019.

[7] T. B. Thiagarajan, S. Ponnusamy, "Effect of cladding of Stellite-6 filler wire on the surface of SS316L alloy through cold metal arc transfer process," J. Met. Mater. Miner., vol. 31, no. 3, pp. 70–84, 2021.

[8] P. Varghese, E. Vetrivendan, M. K. Dash, S. Ningshen, M. Kamaraj, U. K. Mudali, "Weld overlay coating of Inconel 617M on type 316 L stainless steel by cold metal transfer process," Surf. Coat. Technol., vol. 357, pp. 1004–1013, 2019.

[9] A. Evangeline, P. Sathiya, "Cold metal arc transfer (CMT) metal deposition of Inconel 625 superalloy on 316L austenitic stainless steel: microstructural evaluation, corrosion and wear resistance properties," Mater. Res. Express, vol. 6, p. 066516, 2019.

[10] H. Kun, D. Lijin, W. Qinying, Z. Huali, L. Yufei, L. Li, Z. Zhi, "Comparison on the microstructure and corrosion behavior of Inconel 625 cladding deposited by

tungsten inert gas and cold metal transfer process," Surf. Coat. Technol., vol. 435, p. 128245, 2022.

[11] X. Tang, S. Zhang, X. Cui, C. Zhang, Y. Liu, J. Zhang, "Tribological and cavitation erosion behaviors of nickel-based and iron-based coatings deposited on AISI 304 stainless steel by cold metal transfer," J. Mater. Res. Technol., vol. 9, pp. 6665–6681, 2020.

[12] S. Monika, K. Agnieszka, R. Agnieszka, R. Bogdan, "Microstructure, microsegregation and nanohardness of CMT clad layers of Ni-base alloy on 16Mo3 steel," J. Alloys Compd., vol. 751, pp. 86–95, 2018.

[13] G. P. Rajeev, M. Kamaraj, R. S. Bakshi, "Al-Si-Mn alloy coating on aluminum substrate using cold metal transfer (CMT) welding technique," JOM, vol. 66, pp. 1061–1067, 2014.

[14] Z. Bowen, W. Chao, W. Zhaohui, Z. Laiqi, G. Qiang, "Microstructure and properties of Al alloy ER5183 deposited by variable polarity cold metal transfer," J. Mater. Process. Technol., vol. 267, pp. 167–176, 2019.

[15] E. B. Farahani, A. Sarhadi, M. Alizadeh-Sh, S. Fæster, H. Danielsen, M. Eder, "Thermomechanical modeling and experimental study of a multi-layer cast iron repair welding for weld-induced crack prediction," J. Manuf. Process., vol. 104, pp. 443–459, 2023.

[16] M. Jiménez-Xamán, M. Hernández-Hernández, R. Tariq, S. Landa-Damas, M. Rodríguez-Vázquez, A. Aranda-Arizmendi, P. Cruz-Alcantar, "Numerical simulations and mathematical models in laser welding: a review based on physics and heat source models,", Front. Mech. Eng 10:1325623. 2024.https://doi.org/10.3389/fmech.2024.1325623.

[17] R. Escribano-García, N. Rodriguez, O. Zubiri, J. Piccini, I. Setien, "3D numerical simulation of GMAW Cold Metal Transfer using response surface methodology," J. Manuf. Processes, vol. 76, pp. 656–665, 2022.

[18] O. Mokrov, S. Warkentin, L. Westhofen, S. Jeske, J. Bender, R. Sharma, U. Reisgen, "Simulation of wire metal transfer in the cold metal transfer (CMT) variant of gas metal arc welding using the smoothed particle hydrodynamics (SPH) approach," Materialwiss. Werkstofftech., vol. 55, pp. 62–71, 2024.

[19] K. Wu, Z. He, Z. Dong, Y. Lan, "Numerical simulation of the temperature field of cold metal transfer welding pool," MECHANIKA, vol. 22, no. 4, pp. 285–290, 2016.

[20] H. Aberbache, A. Mathieu, N. Haglon, R. Bolot, L. Bleurvacq, A. Corolleur, F. Laurent, "Numerical Study of the Cold Metal Transfer (CMT) Welding of Thin Austenitic Steel Plates with an Equivalent Heat Source Approach," J. Manuf. Mater. Process., vol. 8, p. 20, 2024.

[21] A. S. Azar, "A heat source model for cold metal transfer (CMT) welding," J Therm Anal Calorim 122, pp. 741–746, 2015.

[22] M. Hernández, R. R. Ambriz, A. Amrouche, D. Jaramillo, "Mechanical behavior of dissimilar AL6XN-IN718 welded joint obtained by cold metal transfer," J. Mater. Res. Technol., vol. 30, pp. 1235–1245, 2020.

[23] P. N. Bellamkonda, M. Dwivedy, and R. Addanki, "Cold metal transfer technology - A review of recent research developments," Results in Engineering, vol. 23, p. 102423, 2024.